

See discussions, stats, and author profiles for this publication at: <https://www.researchgate.net/publication/230242987>

# QSAR Analysis of the Anticancer Activity of 2,5-Disubstituted 9-Aza-Anthrapyrazoles

ARTICLE in QSAR & COMBINATORIAL SCIENCE · FEBRUARY 2007

Impact Factor: 1.55 · DOI: 10.1002/qsar.200530216

---

CITATIONS

4

---

READS

36

3 AUTHORS, INCLUDING:



Mariyana Atanasova

Medical University of Sofia

9 PUBLICATIONS 52 CITATIONS

SEE PROFILE



Boris Galabov

Sofia University "St. Kliment Ohridski"

117 PUBLICATIONS 1,309 CITATIONS

SEE PROFILE

# QSAR Analysis of the Anticancer Activity of 2,5-Disubstituted 9-Aza-Anthrapyrazoles

Svetoslav Slavov, Mariyana Atanassova and Boris Galabov\*

Department of Chemistry, University of Sofia, 1 James Bourchier Avenue, 1164 Sofia, Bulgaria, E-mail: galabov@chem.uni-sofia.bg

**Keywords:** Activity, Anticancer, 9-Aza-anthrapyrazoles, DNA binding, Electrostatic interactions, QSAR

Received: December 21, 2005; Accepted: March 25, 2006

DOI: 10.1002/qsar.200530216

## Abstract

The anticancer activity of 35 2,5-disubstituted 9-Aza-Anthrapyrazoles (9-aza-APs) was analyzed employing the Best Multiple Linear Regression (BMLR) as well as a heuristic method for selection of the best descriptors implemented in the CODESSA software to provide a reliable 2D-QSAR model from a set of nearly 500 descriptors. The Chem-X (version 2000) software was used to develop a corresponding 3D-QSAR model. The steric and electrostatic interactions between a probe atom ( $H^+$ ) and a set of aligned molecules were assessed using the comparative molecular field analysis method. The results from 2D- and 3D-QSAR analyses show that the anticancer activity of the studied series of 9-aza-APs is strongly dependent on electrostatic interactions. A binding of these derivatives to DNA has been discussed as a key factor determining the cytotoxic activity against tumor cell. The value of the maximum sum partial negative charge at the nitrogen atoms in 9-aza-APs influences strongly the activity of the compounds. The magnitude of these charges define the hydrogen-bond acceptor properties of the 9-aza-APs. The hydrogen-bond donor properties of the NH and OH groups in the studied series of compounds also play a key role in the binding process. The stable ring structure of the 9-aza-APs also appears to be an important factor for the antitumor activity of the compounds.

## 1 Introduction

The key strategy in the development of antitumor drugs is the design of potential agents that are selectively toxic to the tumor and not to the host organism. The approach to achieve such selectivity is, however, not quite clear and straightforward. Recent studies show that in some cases the anticancer activity correlates with the ability of the agents to influence the speed of DNA cleavage mediated by the enzyme topoisomerase II [1–5]. It is well established that blocking of the topoisomerase II enzyme terminates the further process of DNA replication [1]. It has been shown that the anticancer activity of anthracenedione-based agents is principally correlated with their ability to stimulate DNA cleavage mediated by the topoisomerase II [6]. Drugs from this group possess prominent anticancer properties and find wide clinical application [7–10]. Studies of the mechanism of action of anthraquinone-based derivatives showed that these compounds are able to inhibit the telomerase by folding the telomeric DNA *via* G-quadruplex structures [11, 12]. These structures can be specifically targeted by anthraquinone derivatives. Furthermore, it is established that the anthraquinones are

able to generate radical species that are linked to the cardiac toxicity of compounds from this group [13–15]. Mitoxantrone (MX), an anthracene-9,10-dione (shown in Figure 1), is a drug of the anthracenedione family. MX is an important agent for the treatment of leukemia and lymphomas as well as for the therapy of breast and ovarian cancers [16–18]. The diaminoalkyl groups in the side chains of MX, ametantrone, and other analogues have an essential role for the anticancer effect of these drugs [19, 20]. It is discussed that these derivatives are able to induce interstrand covalent cross-links in DNA of the tumor cells by intercalating into the DNA double helix.

With the aim of developing less toxic agents from the anthracenedione family, new series of aza-anthracenedione derivatives were recently synthesized and tested [2, 21–27]. The presence of nitrogen atom in the planar chromophore of MX affects the cytotoxic activity and the ability to stimulate topoisomerase II-mediated DNA damage in intact cells [28]. Its positioning within the heterocyclic backbone plays a critical role for the activity [2, 21]. Chromophore modification of the anthracenediones related to MX led to the anthrapyrazole class of compounds [29]. Anthrapyrazoles were initially developed with the aim of

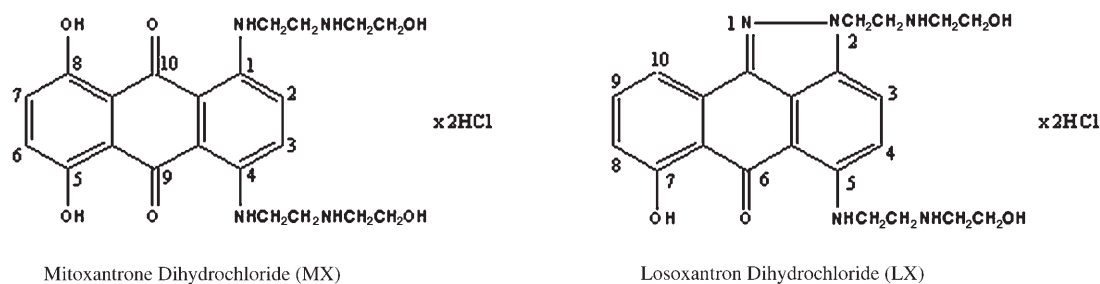


**Figure 1.** Structure of MX and LX.

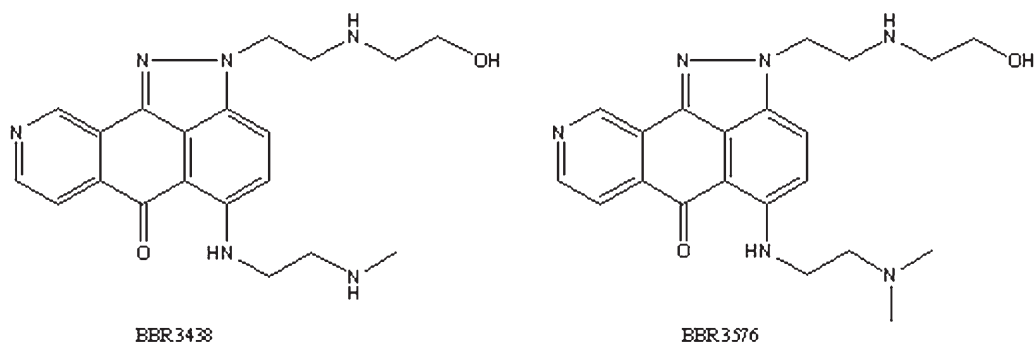


**Figure 2.** Structure of BBR 3438 and BBR 3576.

increasing the spectrum of antitumor activity and reducing the cardiotoxic potential exhibited by the quinone analogues [29–37]. Losoxantrone (LX) (Figure 1), one of anthrapyrazole class of compounds, emerged as the most promising clinical candidate. This compound has demonstrated good clinical efficacy in the treatment of breast cancer but cardiac toxicity was still observed during the clinical trials [30, 38].

In an attempt to minimize the cardiotoxicity of these compounds, *i.e.*, to increase the selectivity, a new series of anticancer aza-anthrapyrazole compounds was recently obtained by Krapcho *et al.* [28]. In particular, the 9-Aza-Anthrapyrazoles (9-aza-APs) seemed to be very promising [28, 39]. *In vitro* evaluation of 9-aza-APs demonstrated high cytotoxic potency against the human colon tumor cell line LoVo and the ability of overcoming multidrug resistance induced in a doxorubicin-resistant cell line [28]. The compounds showed also outstanding *in vivo* antitumor activity against both systemic P388 murine leukemia and MX-1 human mammary carcinoma transplanted in nude mice [28]. These agents are structurally similar to the anthracenedione MX and LX. Their mechanism of action was studied by Sissi *et al.* [40]. The authors showed that the 9-aza-APs exhibit prominent affinity for DNA and established an important electrostatic contribution to the binding free energy. The compounds possess a strong preference for GC base pairs in the double-helical DNA. Their common geometry of complex with DNA is distinguished very much from that of MX. Sissi *et al.* [40] discussed that aza-bioisosteric derivatives of MX and LX do not stimu-

late topoisomerase II-mediated DNA cleavage. This was considered as an indication for alternative, non-enzyme-mediated mechanism(s) for cell killing, possibly related with redox cycling.

On the basis of their efficacy profile in additional experimental tumors and lack of cardiotoxicity in preclinical models [40], two derivatives from the 9-aza-APs family, BBR 3438 (2-[2-(2-hydroxy-ethylamino)-ethyl]-5-(2-methylamino-ethylamino)indazolo [4,3-*g,h*]isoquinoline-6(2*H*)-one) and BBR 3576 (5-(2-(dimethylamino)-ethylamino)-2-[2-(2-hydroxy-ethylamino)-ethyl]-indazolo[4,3-*g,h*] isoquinoline-6(2*H*)-one), have surfaced as potential clinical candidates (Figure 2).

The preclinical profile of efficacy against prostatic carcinoma, a tumor resistant to conventional antitumor drugs, makes the novel 9-aza-AP BBR 3438 a promising candidate for clinical evaluation [41].

The present study aims to gain further insight into the mode of anticancer activity of compounds from the 9-aza-AP series by deriving 2D- and 3D-QSAR models over the series of 35 9-aza-APs synthesized and biologically tested by Krapcho *et al.* [28].

## 2 Methods

### 2.1 Compounds Studied and Biological Activity Data

The compounds analyzed in the present study represent a series of 35 2,5-disubstituted indazolo[4,3-*gh*]isoquinolin-

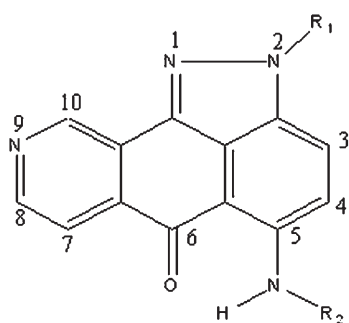


**Figure 3.** General structural formula of 9-aza-APs.

6(2H)-ones with well-expressed cytotoxicity against tumor cell line LoVo. As mentioned, the compounds were synthesized and tested for biological effect by Krapcho *et al.* [28]. The authors showed that their profile of preclinical antitumor activity is comparable to that of MX and is devoid of any significant toxic effect on cardiac tissue, after

both single- and multiple-dose treatments, in rat and mouse [15].

The general formula of the studied aza-anthrapyrazole derivatives is shown in Figure 3. We used the literature data for  $IC_{50}$ , the drug concentration inhibiting 50% of cellular growth following 1 h of drug exposure [28].

The series of compounds studied is presented in Table 1. The original notations of the compounds as introduced by Krapcho *et al.* [28] are retained in the present study. The structure and cytotoxic activity data on LoVo tumor cell line for the studied series of 9-aza-APs are given in Table 1.

## 2.2 Computational Methods

The approach adopted involves two alternative treatments of the anticancer activity data.

(i) QSAR modelling by multilinear regression performed with the CODESSA program [42], which applies to about 500 different constitutional, geometrical, topolog-

**Table 1.** Structures of 2,5-disubstituted 9-aza-APs, and the measured and transformed  $IC_{50}$  values for the series studied.

	$R_1$	$R_2$	$IC_{50}$ ( $\mu\text{mol/L}$ )	$\text{Log}(IC_{50})$
13a	$\text{CH}_2\text{CH}_2\text{N}_2$	$\text{CH}_2\text{CH}_2\text{NMe}_2$	0.925	-0.034
13b	$\text{CH}_2\text{CH}_2\text{NMe}_2$	$\text{CH}_2\text{CH}_2\text{NH}_2$	0.457	-0.340
13c	$\text{CH}_2\text{CH}_2\text{NH}_2$	$\text{CH}_2\text{CH}_2\text{NHMe}$	0.082	-1.084
13d	$\text{CH}_2\text{CH}_2\text{NMe}_2$	$\text{CH}_2\text{CH}_2\text{NHCH}_2\text{CH}_2\text{OH}$	0.507	-0.295
13e	$\text{CH}_2\text{CH}_2\text{NMe}_2$	$\text{CH}_2\text{CH}_2\text{NEt}_2$	0.910	-0.041
13f	$\text{CH}_2\text{CH}_2\text{NMe}_2$	2-(4-morpholinyl)ethyl	3.210	0.506
13g	$\text{CH}_2\text{CH}_2\text{NMe}_2$	$\text{CH}_2\text{CH}_2\text{CH}_2\text{NMe}_2$	0.841	-0.075
13h	$\text{CH}_2\text{CH}_2\text{NMe}_2$	$\text{CH}_2\text{CH}_2\text{CH}_2\text{NH}_2$	4.527	0.656
13i	$\text{CH}_2\text{CH}_2\text{NMe}_2$	2-(1-piperidinyl)ethyl	0.836	-0.078
13j	$\text{CH}_2\text{CH}_2\text{NMe}_2$	2-(1-piperazinyl)ethyl	11.513	1.061
13k	$\text{CH}_2\text{CH}_2\text{NMe}_2$	$\text{CH}_2\text{CH}_2\text{OH}$	0.911	-0.041
13l	$\text{CH}_2\text{CH}_2\text{NMe}_2$	$\text{CH}_2\text{CH}_2\text{N}(\text{CH}_2\text{CH}_2\text{OH})_2$	4.857	0.686
13m	$\text{CH}_2\text{CH}_2\text{NMe}_2$	2-(imidazol-1-yl)ethyl	2.740	0.438
13n	$\text{CH}_2\text{CH}_2\text{NMe}_2$	$\text{CH}_2\text{CH}_2\text{N}(\text{Me})\text{CH}_2\text{CH}_2\text{OH}$	0.120	-0.921
13o	$\text{CH}_2\text{CH}_2\text{NMe}_2$	$\text{CH}_2\text{CH}_2\text{NHSO}_2\text{Me}$	9.568	0.981
13p	$\text{CH}_2\text{CH}_2\text{NMe}_2$	$\text{CH}_2\text{CH}_2\text{NHCH}_2\text{CH}_2\text{NMe}_2$	7.591	0.880
13q	$\text{CH}_2\text{CH}_2\text{NH}_2$	$\text{CH}_2\text{CH}_2\text{NMe}_2$	0.856	-0.067
13r	$\text{CH}_2\text{CH}_2\text{NH}_2$	$\text{CH}_2\text{CH}_2\text{NH}_2$	2.668	0.426
13s	$\text{CH}_2\text{CH}_2\text{NH}_2$	$\text{CH}_2\text{CH}_2\text{NHMe}$	0.624	-0.205
13t	$\text{CH}_2\text{CH}_2\text{NH}_2$	$\text{CH}_2\text{CH}_2\text{NHCH}_2\text{CH}_2\text{OH}$	4.448	0.648
13u	$\text{CH}_2\text{CH}_2\text{NH}_2$	$\text{CH}_2\text{CH}_2\text{NEt}_2$	1.374	0.138
13v	$\text{CH}_2\text{CH}_2\text{NH}_2$	2-(4-morpholinyl)ethyl	4.484	0.652
13w	$\text{CH}_2\text{CH}_2\text{NH}_2$	$\text{CH}_2\text{CH}_2\text{N}(\text{CH}_2\text{CH}_2\text{OH})_2$	113.040	2.053
13x	$\text{CH}_2\text{CH}_2\text{NHCH}_2\text{CH}_2\text{OH}$	$\text{CH}_2\text{CH}_2\text{NMe}_2$	0.761	-0.119
13y	$\text{CH}_2\text{CH}_2\text{NHCH}_2\text{CH}_2\text{OH}$	$\text{CH}_2\text{CH}_2\text{NH}_2$	5.922	0.772
13z	$\text{CH}_2\text{CH}_2\text{NHCH}_2\text{CH}_2\text{OH}$	$\text{CH}_2\text{CH}_2\text{NHMe}$	1.419	0.152
13aa	$\text{CH}_2\text{CH}_2\text{NHCH}_2\text{CH}_2\text{OH}$	$\text{CH}_2\text{CH}_2\text{NHCH}_2\text{CH}_2\text{OH}$	10.963	1.040
13bb	$\text{CH}_2\text{CH}_2\text{NHCH}_2\text{CH}_2\text{OH}$	$\text{CH}_2\text{CH}_2\text{N}(\text{CH}_2\text{CH}_2\text{OH})_2$	219.988	2.342
13cc	$\text{CH}_2\text{CH}_2\text{NHCH}_2\text{CH}_2\text{OH}$	$\text{CH}_2\text{CH}_2\text{OH}$	144.525	2.160
13dd	$\text{CH}_2\text{CH}_2\text{CH}_2\text{NMe}_2$	$\text{CH}_2\text{CH}_2\text{NMe}_2$	0.611	-0.214
13ee	$\text{CH}_2\text{CH}_2\text{CH}_2\text{NMe}_2$	$\text{CH}_2\text{CH}_2\text{NHCH}_2\text{CH}_2\text{OH}$	0.734	-0.134
13ff	$\text{CH}_2\text{CH}_2\text{NHMe}$	$\text{CH}_2\text{CH}_2\text{NHMe}$	0.114	-0.942
13gg	$\text{CH}_2\text{CH}_2\text{NHMe}$	$\text{CH}_2\text{CH}_2\text{NHCH}_2\text{CH}_2\text{OH}$	0.762	-0.118
13hh	$\text{CH}_2\text{CH}_2\text{OH}$	$\text{CH}_2\text{CH}_2\text{NMe}_2$	52.645	1.721
13ii	$\text{CH}_2\text{CH}_2\text{OH}$	$\text{CH}_2\text{CH}_2\text{NH}_2$	88.449	1.947

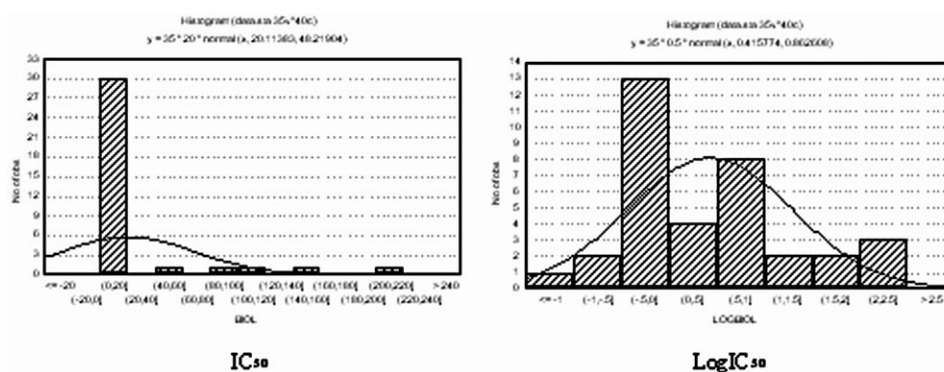


**Figure 4.** Data distribution for  $IC_{50}$  and  $\text{Log } IC_{50}$  values.

ical, electrostatic, and quantum chemical molecular descriptors.

(ii) 3D-QSAR analysis, performed by using the molecular field analysis method as implemented in the Chem-X software [43] combined with Weighted Least Squares (WLS) method for regional mapping.

The distribution of the natural biological activity data ( $IC_{50}$ ) did not correspond to the main statistical requirement for the normal distribution of the data values. Therefore, a logarithmic transformation of data was used, which resulted in a normal distribution curve with the maximum shifted slightly to the left (Figure 4).

As has been noted [44] both 2D- and 3D-QSAR approaches applied to the same series of compounds are expected to provide internally consistent results. 2D-QSAR methods are usually faster, more automated (since they inherently lack the alignment problem), and afford cross-validated  $R^2$  values that are similar or exceed those obtained with 3D- analysis [45].

### 3 Results and Discussion

#### 3.1 2D-QSAR Results

2D-QSAR analysis over the series of 9-aza-APs considered in the present study was carried out by applying the general approach of Hansch [46]. All descriptors used for the purposes of 2D-QSAR were derived solely from molecular structure without reference to experimental data.

The 3D- conversion and preoptimization of molecules were performed using the molecular mechanics force field MM2 as implemented in the Chem3D 5.0 package. The final geometry optimization of the molecules was carried out using the semi-empirical quantum-mechanical AM1 parameterization [47] implemented in the MOPAC program. The optimized structures were loaded into the CODESSA program. Overall, about 500 theoretical descriptors were calculated. These descriptors can be classified into several groups: (i) constitutional, (ii) topological, (iii)

geometrical, (iv) quantum chemical, and (v) charge-related descriptors.

Logarithms of the 1-octanol/water partition coefficient ( $\log P$ ) values were calculated using Clog  $P$  software implemented in the Chem3D program.

An important stage of the multilinear regression QSAR methodology is the search for the best multilinear equation among a given descriptor pool. This process seeks the optimum correlation of the anticancer activity ( $A$ ) with a defined by the user number  $n$  of molecular descriptors ( $D_i$ ), weighted by the regression coefficients  $b_i$ , as given by Eq. 1

$$A = b_0 + \sum_{i=1}^n b_i D_i \quad (1)$$

The heuristic method for selection of the best descriptors and the Best Multiple Linear Regression (BMLR) were used to generate the 2D-QSAR equations involving successively from 1 to 3 descriptors. The best of 3-parameter models (Eq. 2) was selected for the further analysis. Notably, the low number of the descriptors in the equation decreases significantly the chance for a random correlation. The mechanism of action of 2,5-disubstituted 9-aza-APs assigns an important role to electrostatic fields for the observed biological effect [40], in line with this model.

$$\begin{aligned} \log IC_{50} = & 3.25 (\pm 0.99) \text{MACB} + 2470.40 \\ & (\pm 533.85) \text{MPCNA} + 0.10 (\pm 0.02) \text{HDSA-2} - 587.81 \\ & (\pm 221.09) \end{aligned} \quad (2)$$

$$n = 35; R^2 = 0.66; F = 20.25; s^2 = 0.28; Q^2 = 0.56$$

where MACB, Minimum Electron-Nuclear Attraction Energy for a C–C bond; MPCNA, Maximum Partial Charge for a Nitrogen Atom; and HDSA-2, Area-Weighted Surface Charge of Hydrogen-Bonding Donor Atoms.

Removal of six significant outliers (compounds 13j, 13n, 13x, 13cc, 13dd, and 13gg), improved the statistical param-

eters of the model (Eq. 3), but notably, the numerical values of the regression coefficients in the last equation change insignificantly when compared to the 2D-QSAR model for the full dataset.

$$\begin{aligned} \log IC_{50} = & 3.69(\pm 0.53)MACB + 2884.00 \\ & (\pm 303.12)MPCNA + 0.11 (\pm 0.01)HDSA-2 - 662.20 \\ & (\pm 118.59) \end{aligned} \quad (3)$$

$$n = 29; R^2 = 0.90; F = 73.45; s^2 = 0.08; Q^2 = 0.82$$

A comparison of the predicted (by Eq. 3) and experimental  $\log IC_{50}$  values is shown in Figure 5. The positive value of the regression coefficient for the MACB descriptor shows that the larger the value of the descriptor the much stronger are the C–C bonds, *i.e.*, the descriptor correlates with the stability of the carbon framework. MACB is a quantum mechanical energy related descriptor. This energy describes the nuclear-electron driven processes between carbon atoms forming a bond and may be related to the conformational changes of the molecule. In the case of Eq. 3, it describes minimal conformational changes associated with the C–C bonds. The presence of this descriptor in the QSAR equation derived may be linked to the quite stable structure of condensed rings forming the backbone of the series of derivatives treated. Evidently such a stable structure is needed for the compounds to have the antitumor activity discovered. The MPCNA, an electrostatic descriptor, reflects the charge distribution for the nitrogen atoms of the molecule. These atoms are expected to play a critical role in the binding to DNA. The HDSA-2 descriptor is one of the Charged Partial Surface Area (CPSA) descriptors, calculated from MOPAC output partial charges and geometry. This descriptor describes the solvent-accessible surface area of the H-bonding donor atoms. The equation derived suggests a key role of hydrogen bonding in the binding process of the compounds to

the respective sites in DNA. Such a bonding can be realized in two ways: (a) the nucleophilic nitrogen atoms of the 9-aza-APs can act as proton acceptors; (b) the NH or OH functionalities in these molecules can be hydrogen donors. The charges at the nitrogen atoms obviously play an important role for the biological effect of studied compounds. The results obtained are in agreement with the hypothesis of intercalation of the compounds into the DNA molecules. The intercalation can be greatly facilitated by hydrogen bonding.

The efficiency of the QSAR model to predict the  $\log IC_{50}$  value was also estimated using internal cross-validation. The cross-validated correlation coefficient  $Q^2$  was calculated using the leave-one-out procedure as implemented in CODESSA. The correlation coefficients and standard deviations of the linear correlations between experimental and predicted for test sets of  $\log IC_{50}$  values were also calculated (Eqs. 2, 3).

The number of outliers removed to obtain a statistically acceptable 2D-QSAR is relatively large (6 out of 35 compounds). The chemical structure of the outliers does not provide a clue in explaining the exclusion of the respective compounds in the derived model. Other compounds containing similar substituents in chemical nature and size are included in the model. We should note, however, that the effect of each of these outliers on the statistics is not drastic. Typically the removal of each compound brings down the  $R^2$  value by 0.03–0.04. This is an indication that these compounds are not foreign to the derived Eq. 3. Here, one should consider the relatively large experimental error in determining the  $IC_{50}$  values for the treated series. On average it is over 40% but reaches nearly 100% in some cases. Thus, the fluctuations in the experimental activity values can be a serious factor determining the necessity to exclude some compounds from the final derived model (Eq. 3). Otherwise the choice of the optimal descriptors is an objective result of the heuristic method and the BMLR procedure applied. The validity of the derived 2D-QSAR model is strongly supported by the results from the 3D-QSAR analysis as presented in the following section. The 3D-QSAR results strongly support one of the principal conclusions from the 2D- analysis, which underlines a critical role of the electrostatic factors in determining the biological activity of the studied series of compounds. The correlations between the 2D- and 3D-QSAR results will be discussed further in Section 3.2. It should be noted that none of the 35 compounds of the series studied is excluded in the 3D-QSAR treatment.

### 3.2 3D-QSAR Results

In order to achieve consistent results, a similar computational procedure was applied for each molecule. For the correct guess of the 3D- geometry, the conformational space of each compound was searched using the systematic search method implemented in the Chem-X program. All

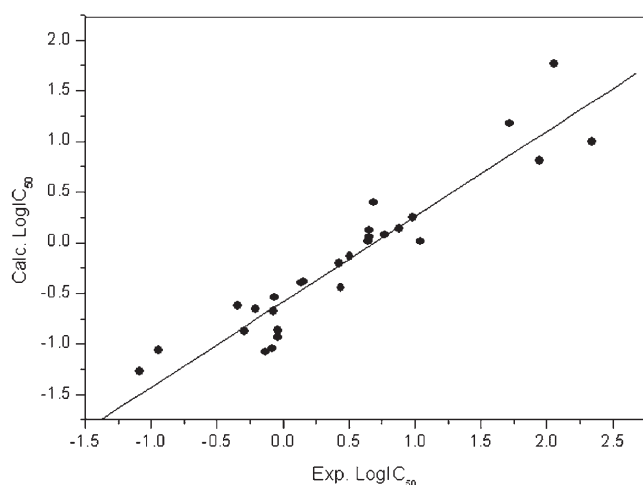


**Figure 5.** Experimental vs. calculated values for  $\log IC_{50}$  values.



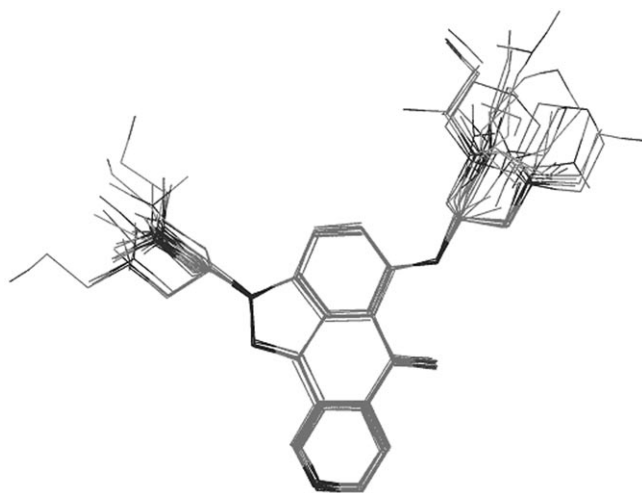


**Figure 6.** Aligned molecules from the series.

the single bonds were rotated to 180° using a 30° step. In the case of double bonds both *cis*- and *trans*-conformers were considered. All generated structures with improper Van der Waals contacts were excluded from the calculations. The energy was computed using molecular mechanics with the AMBER force field [48]. The conformers with lowest energy were additionally optimized by the MOPAC program as implemented in Chem-X software using the AM1 semiempirical quantum mechanical method.

An important step for a correct 3D-QSAR analysis is the selection of a proper structure for superimposing the molecules. According to the key-lock principle in 3D-QSAR [49], the most active compound in the series should have a geometry nearest to optimal for the ligand–receptor interactions. For this reason, we chose the compound **13c** (2-[2-(dimethylamino)ethyl]-5-[[2-(methylamino)ethyl]-amino]indazolo[4,3-*g,h*]isoquinolin-6(2H)-one dimaleate) as the template for aligning all the remaining molecules.

Flexible fitting procedures as implemented in Chem-X were employed to superimpose all molecules from the series (Figure 6). Our field comparisons with flexible fitted structures are based on calculated Root Mean Square (RMS) errors, where the entire conformational space was explored in searching molecules with minimum RMS between them and molecule **13c**. Only a single conformer for each molecule was used – the one that best fits the template.

The next step was to build a 3D- grid around the set of superimposed molecules using a 1 Å grid constant. The probe atom was H<sup>+</sup>. The grid space is with 4 Å bigger than the size of the largest molecules. The steric and electrostatic interaction energies between the probe atom and the set of aligned molecules were calculated for each grid-point using 0.95 cut-offs default for both fields.

The two-pass Partial Least Squares (PLS) method was used to obtain the 3D-QSAR model. The first step in this

method was to calculate the Principal Components (PCs) and the second was to obtain the model and its statistical parameters. Six PCs for both the steric and electrostatic interaction energies were generated. A separate covariance matrix was constructed from the data table. PLS determines the full eigensystem of this matrix using the Singular Value Decomposition (SVD) method. The matrix was rewritten in a new form, and the coefficients of the transformed variables (the PC loadings) were evaluated and used to determine the PC scores, a set of new variables which best explain the variance in the data.

For the steric and electrostatic fields the calculated PCs cover over 80% of the data dispersion. As a measure of the internal predictive power of the model the following parameters were used: the correlation coefficient  $R^2$ , the cross-validated correlation coefficient  $Q^2$ , and the internal predictive correlation coefficient  $R^2_{\text{pred}}$ .  $Q^2$  was computed employing the leave-group-out procedure using randomly generated sixth subgroups of the training set. To evaluate the external predictive power of the model, the dataset was divided randomly into two parts by using the rule of the equal distribution of the biological activity data in the training and the test sets. Using the test series  $R^2_{\text{ext}}$  was calculated.

By using the WLS method implemented in Chem-X,  $R^2$  maps were generated separately for the steric and electrostatic fields. The portions of the normal coordinate space where the variation in map data values relates to activity were visualized. An  $R^2$  map was generated by discarding those points, which do not correlate with the activity, and storing the  $R^2$  value of the correlation for each remaining point.

### 3.2.1 Results for Steric Fields

In the case of steric interaction energies, the initial dataset consisting of 35 compounds was randomly separated into two groups – respectively 24 compounds for the training set and 11 compounds for the test set. The best obtained final model is given below.

#### Training Set

$$\log \text{IC}_{50} = 0.066(\text{CP1}) + 0.040(\text{CP2}) + 0.092(\text{CP3}) + 0.371 \quad (4)$$

$$n = 24; R^2 = 0.67; R^2_{\text{pred}} = 0.65; Q^2 = 0.38; s = 1.01$$

#### Test Set

$$n = 11; R^2_{\text{ext}} = 0.06$$

Two-pass PLS method was used to compute  $R^2$ ,  $R^2_{\text{pred}}$ , and  $Q^2$  values. The final model obtained is written in terms of the PCs generated by PLS. In the equation shown above, the PCs are denoted by CPX ( $X=1-3$ ). The difference between  $R^2$  and  $Q^2$  values defines the internal predictive

power of the model. As can be seen,  $R^2$  is about two times bigger than the  $Q^2$  value. The result indicates that the model is not satisfactory from the statistical viewpoint. Thus, the steric interactions do not appear to have a major role in explaining the biological activity of the compounds. The conclusion is fully supported by statistical data obtained from the test series, where  $R^2_{\text{ext}}$  has a very low value. The very stable structure of the backbone 9-aza-AP is, evidently, essential for the biological activity. On the other hand, the backbone structure is too rigid to be influenced substantially by steric effects of the substituents around the ring system.

### 3.2.2 Results for Electrostatic Fields

An analogous approach was used to evaluate the effect of electrostatic interactions over the biological activity. The final model (Eq. 5) obtained has the following form and statistical parameters.

#### Training Set

$$\log \text{IC}_{50} = 0.153(\text{PC1}) + 0.058(\text{PC2}) + 0.036(\text{PC3}) + 0.393 \quad (5)$$

$$n = 26; R^2 = 0.96; R^2_{\text{pred}} = 0.94; Q^2 = 0.69; s = 0.89$$

#### Test Set

$$n = 9; R^2_{\text{ext}} = 0.66$$

As in the case of steric fields the model is written in terms of the PLS generated by PCs – PCX ( $X = 1-3$ ). As mentioned above, the  $R^2 - Q^2$  difference defines the internal predictive power of the model. It is seen that in this case it is much higher than for the steric interactions. The obtained  $R^2_{\text{ext}}$  value for the test series also proved the model validity and quality. It can be concluded that the electrostatic interactions have a significant role in defining the observed anticancer effect of 9-aza-APs. This result is in full accord with the 2D-QSAR data as presented in Eqs. 2, 3. As discussed, two of the descriptors included in these equations play a critical role for the electrostatic interactions determining the binding to DNA. The WLS map shows the important parts for the electrostatic interaction from the unexplored parametric space around the set of the superimposed molecules (Figure 7). As seen from Figure 7, the presence of aliphatic substituents containing an amino group in the second position, hydrocarbon residues containing strongly electronegative atoms in the fifth position as well as a keto group in the sixth position of the heterocyclic system lead to increased biological activity.

The WLS map shows that positions seven, eight, and nine (on Figure 7) also contribute to the biological data explanation. This hypothesis is also supported by the results of Krapcho *et al.* [28] who synthesized some additional

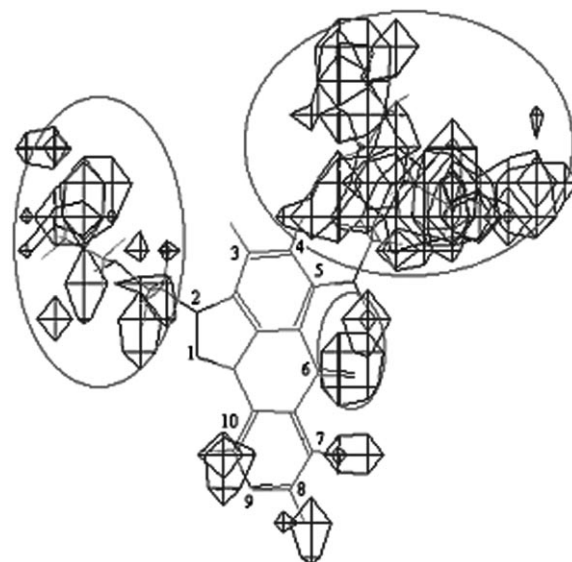


**Figure 7.** WLS  $R^2$  map for the electrostatic interactions visualized over the structure of molecule 13c. The encircled parts show the important regions for the anticancer activity.

structures with nitrogen atoms at these positions and found out that these molecules have similar biological effect. As can be seen, the 3D- electrostatic isosurface around the ninth position is bigger than others and this should be the most preferable place for the nitrogen. The same conclusion for the position of the heterocyclic nitrogen has been obtained from the experimental biological tests [28].

The established 2D- and 3D-QSAR models for the studied series of 9-aza-APs are both: (i) in accordance with the probable mechanism of action of 2,5-disubstituted 9-aza-APs discussed in terms of the available experimental data [40], and (ii) compatible with each other. The results of the calculations presented in this work show clearly that the electrostatic interactions have a decisive role in determining the cytotoxic activity of the compounds against the human colon tumor cells line LoVo. These results are in accord with the experimental finding of Sissi *et al.* [40] regarding the importance of electrostatic interactions for the binding of 9-aza-APs to DNA. The stable ring structure of the derivatives is also an important factor for the antitumor activity of the studied 9-aza-APs.

The 3D- results obtained regarding the structural features of potentially active compounds can be summarized as follows:

- (i) The presence of an aliphatic substituent containing an amino group in the second position of the heterocyclic system has a positive effect on the biological activity.
- (ii) The presence of a hydrocarbon residue in the fifth position containing strongly electronegative elements such as oxygen in different functional groups, for example carbonyl group, would increase the cytotoxic activity against tumor cell line LoVo.



(iii) A keto group in the sixth position contributes to higher activity of the studied compounds.

(iv) The presence of a nitrogen atom in the ninth position is also important for the activity.

(v) The non-flexible ring structure of the compounds appears also as a factor linked to the antitumor activity.

## 4 Conclusions

The results from 2D- and 3D-QSAR analyses show that the anticancer activity of the studied series of 9-aza-APs is strongly dependent on electrostatic interactions. A binding of these derivatives to DNA has been discussed as a key factor determining the cytotoxic activity against tumor cells. The value of the maximum sum partial negative charge at the nitrogen atoms in 9-aza-APs is influencing strongly the activity of the compounds. The magnitude of these charges define the hydrogen-bond acceptor properties of the 9-aza-APs. The hydrogen-bond donor properties of the NH and OH groups in the studied series of compounds play also a key role in the binding process. The stable ring structure of the 9-aza-APs appears also to be an important factor for the antitumor activity of the compounds.

## Acknowledgements

The authors thank Professor M. Karelson, University of Tartu, for making available the CODESSA software package.


## References

- [1] H. Malonne, G. Atassi, *Anticancer Drugs* **1997**, *8*, 811–822.
- [2] A. P. Krapcho, M. J. Maresch, M. P. Hacker, L. Hazlehurst, E. Menta, A. Oliva, S. Spinelli, G. Beggiolin, F. C. Giuliani, G. Pezzoni, S. Tognella, *Curr. Med. Chem.* **1995**, *2*, 803–824.
- [3] F. Arcamone, S. Penco, Synthesis of New Doxorubicin Analogs, in: J. W. Lown (Ed.), *Anthracycline and Anthracenedione-based Anticancer Agents*, Elsevier, New York, **1988**.
- [4] R. K. Y. Zee-Cheng, C. C. Cheng, *Drugs Future* **1983**, *8*, 229–248.
- [5] S. K. Sengupta, Topoisomerase II Inhibitors, in: W. O. Foye (Ed.), *Cancer Chemotherapeutic Agents*, American Chemical Society, Washington DC, **1995**, pp. 205–260.
- [6] H. Malonne, G. Atassi, *Anticancer Drugs* **1997**, *8*, 811–822.
- [7] G. N. Hortobagyi, *Drugs* **1997**, *54* (Suppl. 4), S1–S7.
- [8] X. Thomas, E. Archimbaud, *Hematol. Cell. Ther.* **1997**, *39*, 63–74.
- [9] L. R. Wiseman, C. M. Spencer, *Drugs Aging* **1997**, *10*, 473–485.
- [10] F. M. Arcamone, *Biochimie* **1998**, *80*, 201–206.
- [11] P. J. Perry, S. M. Gowan, A. P. Reszka, P. Polucci, T. C. Jenkins, L. R. Kelland, S. Neidle, *J. Med. Chem.* **1998**, *41*, 3253–3260.
- [12] P. J. Perry, M. A. Read, R. T. Davies, S. M. Gowan, A. P. Reszka, A. A. Wood, L. R. Kelland, S. Neidle, *J. Med. Chem.* **1999**, *42*, 2679–2684.
- [13] W. H. Frishman, H. M. Sung, H. C. Yee, L. L. Liu, D. Keefe, A. I. Einzig, J. Dutcher, *Curr. Probl. Cancer* **1997**, *21*, 301–360.
- [14] A. Giantris, L. Abdurrahman, A. Hinkle, B. Asselin, S. E. Lipshultz, *Crit. Rev. Oncol. Hematol.* **1998**, *27*, 53–68.
- [15] A. Liwo, D. Jeziorek, T. Ossowski, D. Dyl, A. Tempczyk, J. Tarasuik, M. Nowacka, E. Borowski, W. Woznicki, *Acta Biochem. Pol.* **1995**, *42*, 445–456.
- [16] D. Flauds, J. A. Balfour, P. Chrisp, H. D. Langtry, *Drugs* **1991**, *41*, 400–449.
- [17] C. J. Dunn, K. L. Goa, *Drugs Aging* **1996**, *9*, 122–147.
- [18] L. R. Wiseman, C. M. Spencer, *Drugs Aging* **1997**, *10*, 473–485.
- [19] A. Składanowski, J. Konopa, *Br. J. Cancer* **2000**, *82*, 1300–1304.
- [20] C. C. Cheng, R. K. Y. Zee-Cheng, The Design, Synthesis, and Development of a New Class of Potential Antineoplastic Anthraquinones, in: G. P. Ellis, G. B. West (Eds.), *Progress in Medicinal Chemistry*, Elsevier, New York, **1989**, pp. 83–118.
- [21] A. P. Krapcho, M. E. Petry, Z. Getahun, J. J. Landi, Jr., J. Stallman, J. F. Polsenberg, C. E. Gallagher, M. J. Maresch, M. P. Hacker, F. C. Giuliani, G. Beggiolin, G. Pezzoni, E. Menta, C. Manzotti, A. Oliva, S. Spinelli, S. Tognella, *J. Med. Chem.* **1994**, *37*, 828–873.
- [22] L. A. Hazlehurst, A. P. Krapcho, M. P. Hacker, *Biochem. Pharmacol.* **1995**, *50*, 1087–1094.
- [23] L. A. Hazlehurst, A. P. Krapcho, M. P. Hacker, *Cancer Lett.* **1995**, *91*, 115–124.
- [24] P. De Isabella, M. Palumbo, C. Sissi, G. Capranico, N. Carenini, E. Menta, A. Oliva, S. Spinelli, A. P. Krapcho, F. C. Giuliani, F. Zunino, *Mol. Pharmacol.* **1995**, *48*, 30–38.
- [25] C. Sissi, G. Capranico, E. Menta, M. Palumbo, *Mol. Pharmacol.* **1996**, *50*, 838–845.
- [26] P. De Isabella, M. Palumbo, C. Sissi, N. Carenini, G. Capranico, E. Menta, A. Oliva, S. Spinelli, A. P. Krapcho, F. C. Giuliani, F. Zunino, *Biochem. Pharmacol.* **1997**, *53*, 161–169.
- [27] C. Sissi, S. Moro, A. P. Krapcho, E. Menta, M. Palumbo, *Anticancer Drug Des.* **1999**, *14*, 265–274.
- [28] A. P. Krapcho, E. Menta, A. Oliva, R. Di Domenico, L. Fiocchi, E. Maresch, C. E. Gallagher, M. P. Hacker, G. Beggiolin, F. C. Giuliani, G. Pezzoni, S. Spinelli, *J. Med. Chem.* **1998**, *41*, 5429–5444.
- [29] H. D. H. Showalter, J. L. Johnson, J. M. Hoftiezer, W. R. Turner, L. M. Werbel, W. R. Leopold, J. L. Shillis, R. C. Jackson, E. F. Elslager, *J. Med. Chem.* **1987**, *30*, 121–131.
- [30] D. C. Talbot, I. E. Smith, J. L. Mansi, I. Hudson, A. H. Calvert, S. E. Ashley, *J. Clin. Oncol.* **1991**, *9*, 2141–2147.
- [31] E. Cavalletti, L. Crippa, O. Bellini, E. Menta, R. Cavagnoli, D. Delbo, *Proc. Am. Assoc. Cancer Res.* **1993**, *34*, Abstr 2227.
- [32] L. H. Patterson, D. R. Newell, Cellular and Molecular Pharmacology of the Anthrapyrazole Antitumour Agents, in: S. Neidle, M. Waring (Eds.), *Molecular Aspects of Anticancer Drug-DNA Interactions*, Macmillan, New York, **1994**, pp. 96–129.
- [33] I. R. Judson, *Anticancer Drugs* **1991**, *2*, 223–231.
- [34] H. Gogas, J. L. Mansi, *Cancer Treat. Rev.* **1995**, *21*, 541–552.
- [35] S. Berg, *Crit. Rev. Oncol./Hematol.* **1996**, *22*, 79–87.

- [36] G. N. Hortobagyi, *Semin. Oncol.* **1997**, 24(Suppl. 17), S17-1–S17-4.
- [37] M. Barbu, N. Azarnia, H. Calvert, *Ann. Oncol.* **1994**, 5(Suppl. 5), Abstr 288.
- [38] S. M. Walsh, W. M. Walley, M. Chandra, S. D. Huan, J. P. Veinot, L. A. J. Higginson, *Can. J. Cardiol.* **1995**, 11, 419–422.
- [39] A. P. Krapcho, E. Menta, *Drugs Future* **1997**, 22, 641–646.
- [40] C. Sissi, S. Moro, S. Richter, B. Gatto, E. Menta, S. Spinelli, A. P. Krapcho, F. Zunino, M. Palumbo, *Mol. Pharmacol.* **2001**, 59, 96–103.
- [41] R. Supino, D. Polizzi, R. Pavesi, G. Pratesi, F. Guano, G. Capranico, M. Palumbo, C. Sissi, S. Richter, G. Beggiolin, E. Menta, G. Pezzoni, S. Spinelli, D. Torriani, N. Carenini, L. Dal Bo, F. Facchinetti, M. Tortoreto, F. Zunino, *Oncology* **2001**, 61, 234–242.
- [42] A. R. Katritzky, V. S. Lobanov, M. Karelson (Eds.), *CODESSA: Reference manual (version 2.0)*, Gainesville, Florida, **1994**.
- [43] Chem-X, Chem-X was developed at Chemical Design Ltd. (now part of Accelrys), **1998**.
- [44] I. C. Muszynski, L. Scapozza, K.-A. Kovar, G. Folkers, *Quant. Struct.-Act. Relat.* **1999**, 18, 342–353.
- [45] Z. Weifan, E. Ganesh Srinivas, C. Sung Jin, A. Tropsha, *215th ACS National Meeting, Comparative studies of 3D (CoMFA) and 2D QSAR methods, Book of Abstracts*, American Chemical Society, Washington, **1998**.
- [46] C. Hansch, A. Leo, *Fundamentals and Applications in Chemistry and Biology*, in: S. R. Heller, (Ed.), *Exploring QSAR*, American Chemical Society, Washington, DC, **1995**.
- [47] M. J. S. Dewar, E. G. Zoebisch, E. F. Healy, J. J. P. Stewart, *J. Am. Chem. Soc.* **1985**, 107, 3902–3909.
- [48] U. C. Singh, P. K. Weiner, J. Caldwell, P. A. Kollman, *AMBER Version 3*, University of California, San Francisco.
- [49] H. Kubinyi, *Pharm. Acta Helv.* **1995**, 69, 259–269.

Since 1807...

# Wiley



# Knowledge for Generations

BICENTENNIAL  
**1807**  
BICENTENNIAL  
**WILEY**  
BICENTENNIAL  
**2007**  
BICENTENNIAL  
[wiley.com](http://wiley.com)